

# PKS 1830–211: A Face-On Spiral Galaxy Lens

Joshua N. Winn<sup>1</sup>, Christopher S. Kochanek<sup>1</sup>, Brian A. McLeod<sup>1</sup>, Emilio E. Falco<sup>2</sup>,  
Christopher D. Impey<sup>3</sup>, Hans-Walter Rix<sup>4</sup>

## ABSTRACT

We present new Hubble Space Telescope images of the gravitational lens PKS 1830–211, which allow us to characterize the lens galaxy and update the determination of the Hubble constant ( $H_0$ ) from this system. The  $I$ -band image shows that the lens galaxy is a face-on spiral galaxy with clearly delineated spiral arms. The southwestern image of the background quasar passes through one of the spiral arms, explaining the previous detections of large quantities of molecular gas and dust in front of this image. The lens galaxy photometry is consistent with the Tully-Fisher relation, suggesting the lens galaxy is a typical spiral galaxy for its redshift. The lens galaxy position, which was the main source of uncertainty in previous attempts to determine  $H_0$ , is now known precisely. Given the current time delay measurement and assuming the lens galaxy has an isothermal mass distribution, we compute  $H_0 = 44 \pm 9 \text{ km s}^{-1} \text{ Mpc}^{-1}$  for an  $\Omega_m = 0.3$  flat cosmological model. We describe some possible systematic errors and how to reduce them. We also discuss the possibility raised by Courbin et al. (2002), that what we have identified as a single lens galaxy is actually a foreground star and two separate galaxies.

*Subject headings:* quasars: individual (PKS 1830–211)—gravitational lensing—cosmology: distance scale

---

<sup>1</sup>Harvard-Smithsonian Center for Astrophysics, 60 Garden St., Cambridge, MA 02138; jwinn, kochanek, bmcleod@cfa.harvard.edu

<sup>2</sup>Smithsonian Institution, Whipple Observatory, 670 Mt Hopkins Road, P.O. Box 97, Amado, AZ 85645; falco@cfa.harvard.edu

<sup>3</sup>Steward Observatory, University of Arizona, Tucson, AZ 85721; cimpey@as.arizona.edu

<sup>4</sup>Max-Planck-Institut für Astronomie, Königsstuhl 17, D-69117 Heidelberg, Germany; rix@mpia-hd.mpg.de

## 1. Introduction

Although the Hubble Space Telescope (HST) Key Project to Measure the Hubble Constant has been successfully completed (Freedman et al. 2001), it is important to pursue completely different methods of determining the Hubble constant ( $H_0$ ). Independent methods provide a consistency check, and may eventually surpass the 10% accuracy of the local distance-scale methods employed by the Key Project. It is also important to measure the expansion rate directly at cosmological redshifts, in case the Galaxy is in a locally underdense or overdense region (see, e.g., Wu et al. 1995). These goals will grow in importance in the coming years due to the degeneracies in analyses of cosmic microwave background anisotropies between many cosmological parameters and  $H_0$  (e.g., Bond et al. 1994; Eisenstein, Tegmark, & Hu 1998).

A promising approach to determining  $H_0$  that is independent of the local distance scale uses gravitational lens time delays (Refsdal 1964; for recent summaries see, e.g., Schechter 2000, Koopmans & Fassnacht 1999). This method is ultimately limited by systematic uncertainties in the mass models of the lens galaxies, but a necessary first step is to obtain the basic observational constraints—astrometry, photometry, and redshifts of the lens and source—for the systems with measured time delays.

For the gravitational lens PKS 1830–211, this has been especially challenging because the system is near the Galactic plane ( $b = -5^\circ.7$ ). As a result, most of the information has come from radio and infrared observations. Rao & Subrahmanyan (1988) suggested it was a lens due to its radio morphology. Subrahmanyan et al. (1990) and Jauncey et al. (1991) provided more conclusive evidence; the system has two bright point sources (NE and SW) embedded in a fainter Einstein ring. Strong molecular absorption features were detected at  $z_l = 0.886$  (Wiklind & Combes 1996; Gerin et al. 1997), largely in front of SW (Frye, Welch, & Broadhurst 1997; Swift, Welch, & Frye 2001), and presumably due to the lens galaxy. Lovell et al. (1996) found  $z_a = 0.19$  H I absorption in front of NE, of unknown provenance. Lovell et al. (1998) measured a time delay of  $26_{-5}^{+4}$  days between NE and SW at 8.6 GHz. By deconvolving ground-based infrared images, Courbin et al. (1998) detected the quasar images and found hints of the lens galaxy. Lidman et al. (1999) determined the quasar redshift of  $z_s = 2.507$  by infrared spectroscopy. From the presence and structure of the molecular absorption system, Wiklind & Combes (1998) argued that the lens galaxy is probably a spiral galaxy seen nearly face-on, which is consistent with the large differential extinction between NE and SW ( $\Delta E_{B-V} \approx 3$ ) observed by Falco et al. (1999). However, although Lehár et al. (2000) detected the lens galaxy in  $H$ -band and shallow  $I$ -band HST images, they could not determine its position or structure accurately. These authors found that the uncertainty in the lens galaxy position dominated the uncertainty in the value of

$H_0$  inferred from the time delay.

In this paper we present new HST optical images that confirm the lens galaxy is a face-on spiral galaxy, and allow its position and optical magnitudes to be measured accurately. These data are discussed in § 2. In § 3, we place the lens galaxy on the Tully-Fisher relation using the HST photometry and two different estimators of the galaxy mass—one from the lens geometry, and one from the velocity shift measured by Wiklind & Combes (1998). In § 4, we incorporate our measurement of the position of the lens galaxy into a simple lens model to arrive at an updated estimate of  $H_0$ . We also discuss systematic errors and compare our model with previous models.

After this work was completed, we learned that Courbin et al. (2002) independently analyzed the same HST data, along with new and archival near-IR data. They argue that what we have identified as the bulge of the lens galaxy is actually a foreground star, and that there is a second lens galaxy. In the final section of this paper, we describe the strengths, weaknesses, and future tests of these competing hypotheses, and discuss future prospects for reducing systematic errors in  $H_0$  from this particular gravitational lens.

## 2. Observations and data reduction

PKS 1830–211 was observed with HST/WFPC2<sup>5</sup> on 2000 September 25 with the F814W filter, using 4 dithered exposures, for a total integration time of 4800 s. On 2001 July 11 it was observed with the F555W filter, using 3 dithered exposures, for a total integration time of 2000 s. In both cases PKS 1830–211 was centered on the PC chip. We cross-registered and combined the exposures, and rejected cosmic rays, using the Drizzle algorithm implemented in IRAF (Fruchter & Hook 2002).

Figure 1 shows the F814W (hereafter “*I*-band”) image. The lens galaxy, labeled G, is a nearly face-on spiral galaxy (probably an Sb or Sc). The bulge of the galaxy is detected with high significance and is compact. The position of quasar SW (as determined from radio images) is covered by one of the spiral arms. Object S1 is an M star identified by Djorgovski et al. (1992), and G2 is a galaxy identified by Lehár et al. (2000). Inset in the upper right corner of the image is a contour map of G, based on the same data, that shows the western spiral arm more clearly than the grayscale image. Figure 2 shows the F555W (hereafter “*V*-band”) image. In this image the bulge of G is only marginally detected.

---

<sup>5</sup>Data from the NASA/ESA Hubble Space Telescope (HST) were obtained from the Space Telescope Science Institute, which is operated by AURA, Inc., under NASA contract NAS 5-26555.

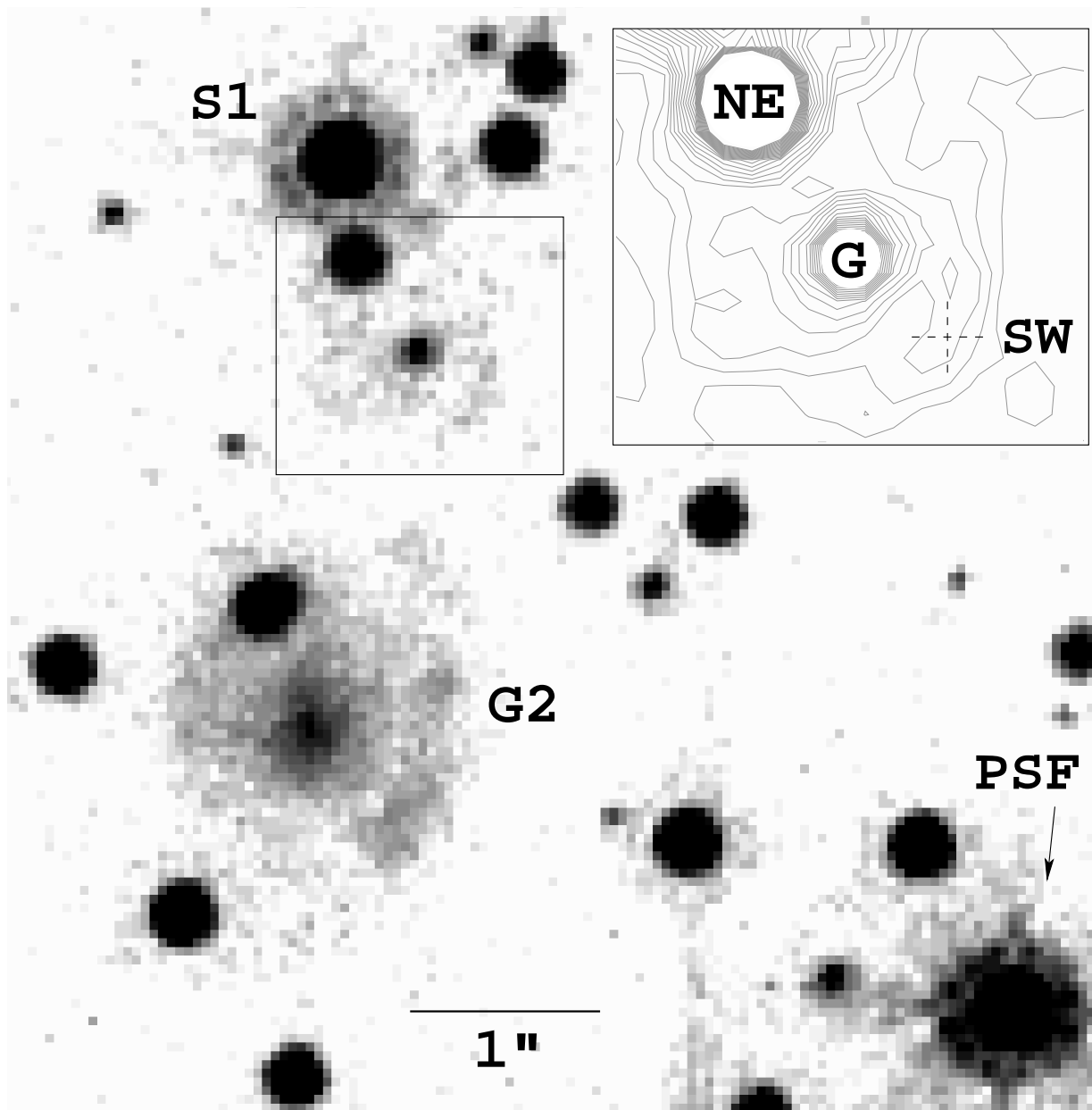


Fig. 1.— HST/WFPC2 image, filter F814W  $\approx I$ . North is up and east is left. Note that  $1''$  corresponds to  $5.4h^{-1}$  kpc at the lens redshift (in a flat  $\Omega_m = 0.3$  cosmology). Inset in the upper right of the image is a contour representation of the region surrounding G, based on the same data. The position of SW, as determined from radio images, is marked.

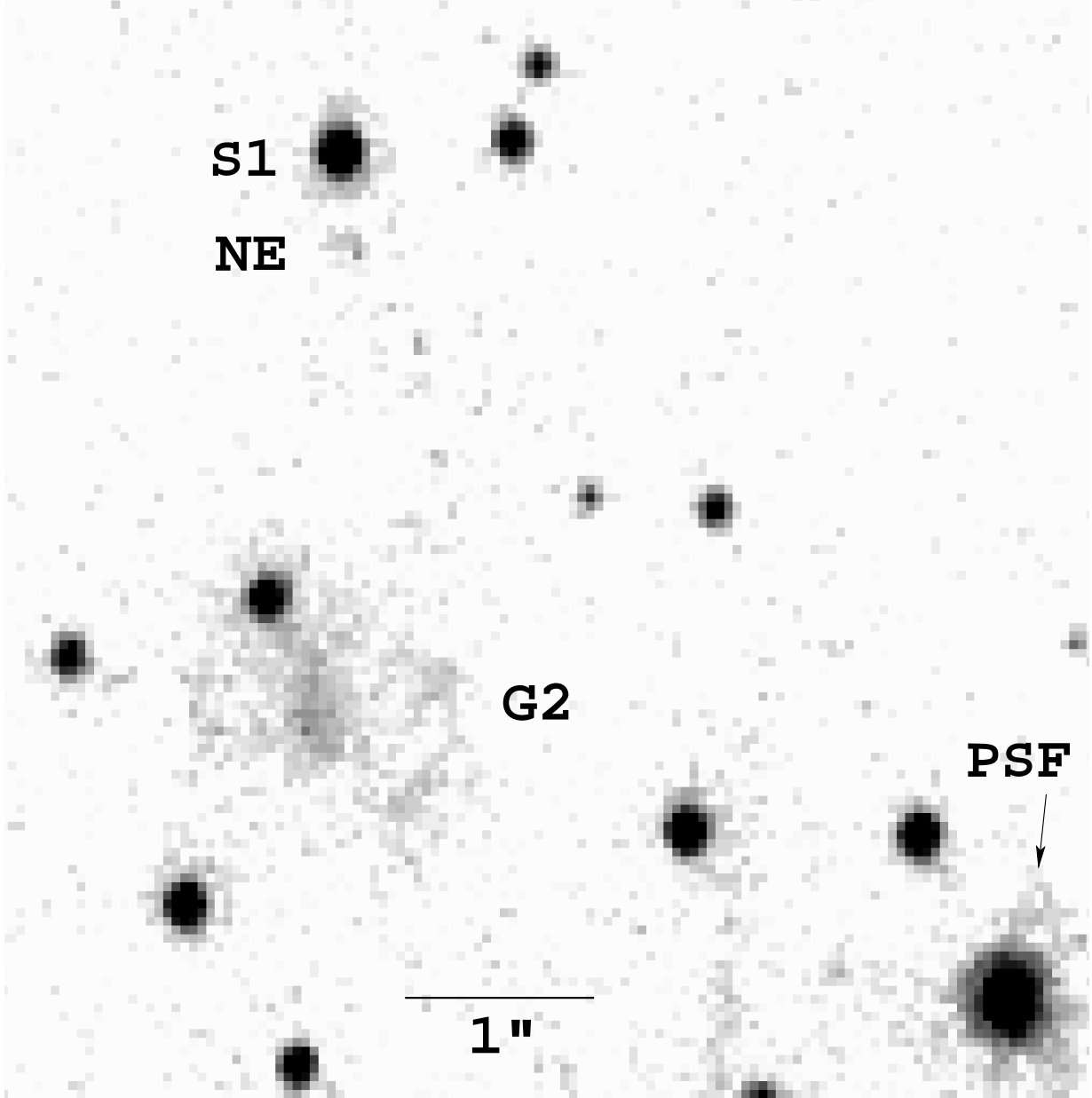


Fig. 2.— HST/WFPC2 image, filter F555W  $\approx V$ . North is up and east is left. Note that  $1''$  corresponds to  $5.4h^{-1}$  kpc at the lens redshift (in a flat  $\Omega_m = 0.3$  cosmology).

To measure the position of G relative to NE, which is the crucial quantity for modeling purposes, we used software written for the Center for Astrophysics–Arizona Space Telescope Lens Survey (CASTLES; see, e.g., Lehár et al. 2000) to fit a parameterized model to the *I*-band image. A well-exposed star  $3''.43$  west and  $3''.94$  south of NE was used as an empirical PSF. (Although this star might appear overexposed in Figures 1 and 2, this is due only to the chosen scaling of gray levels.)

Our model consisted of point sources representing: S1, NE, the central bulge of G, and all stars within  $5''$  of NE. We estimate the uncertainty in each coordinate of the G–NE separation to be 4 milliarcseconds, which is the variance of the separations obtained by individually fitting the four *I*-band exposures. The result did not change significantly when the empirical PSF was replaced by a theoretical “Tiny Tim” PSF (Krist & Hook 1997), nor when G was represented as a Gaussian or de Vaucouleurs profile instead of a point source. The results are given in Table 1, which also summarizes the basic data for PKS 1830–211 drawn from this work and the literature.

We applied the same model to the *V*-band image, but fixed the relative positions at the *I*-band values and allowed only the fluxes to vary. The fluxes of the point sources were converted to magnitudes using the zero points and CTE correction formulae of Dolphin (2000)<sup>6</sup>. The results are given in Table 2. The quoted error is the quadrature sum of the variance obtained by fitting the separate exposures, and 0.04 due to PSF subtraction. They do not include an overall uncertainty of  $\sim 0.05$  due to zero points and CTE correction.

Because neither G nor G2 is well described by an analytic profile, we measured the magnitude of each galaxy within a synthetic circular aperture, using an image with all the point sources subtracted (except the point source representing the bulge of G). In particular, two point sources were subtracted on the northeast edge of G2, to represent what appears to be a pair of blended stars. For G, the aperture radius was  $0''.7$ ; for G2, it was  $1''$ . No CTE correction was made because the correction procedure for extended sources is unknown and the correction is probably small (Riess 2000). The errors quoted in Table 2 are due to uncertainty in the sky level and contributions from the residuals of the neighboring point sources.

---

<sup>6</sup>As updated on the web site of A. Dolphin, <http://www.nao.edu/staff/dolphin/wfpc2.calib/>, referenced 2001 November 15.

### 3. The lens galaxy luminosity and the Tully-Fisher relation

The Tully-Fisher relation is an empirical correlation between the luminosity and mass of disk galaxies that has been observed for both nearby galaxies (see, e.g., Tully & Fisher 1977; Sakai et al. 2000) and for galaxies at significant redshifts (e.g., Vogt et al. 1996, 1997; Ziegler et al. 2001). Typically, the measure of luminosity is rest-frame  $M_B$  and the measure of mass is the circular rotation velocity. For most galaxies at  $z \sim 1$  the latter measurement is a challenging spectroscopic project, especially for a nearly face-on spiral galaxy. Lens galaxies are special because an accurate mass measurement is available from the geometry of the background images. Given the HST photometry and image configuration of PKS 1830–211, we can attempt to place the lens galaxy on the Tully-Fisher relation.

We corrected the  $I$ -band magnitude of the lens galaxy for Galactic extinction using the  $E_{B-V}$  value of Schlegel, Finkbeiner, & Davis (1998) and assuming a  $R_V = 3.1$  extinction law, obtaining  $A_I = 0.81$ . For the lens redshift  $z_l = 0.886$ , the  $I$ -band is nearly centered on the rest-frame  $B$ -band, so there is little uncertainty in the  $k$ -correction:  $B_{\text{rest}} - I \approx 1.05 \pm 0.05$  mag. For a flat  $\Omega_m = 0.3$  cosmology with  $H_0 = 65$  km s<sup>−1</sup> Mpc<sup>−1</sup>, the implied rest-frame absolute magnitude of the lens galaxy is  $M_B = -21.7 \pm 0.3$  mag, with the quoted uncertainty entirely due to the measurement error. We attempt no extrapolation from our aperture magnitude to a total magnitude, nor do we correct for internal extinction, so the resulting luminosity should be an underestimate.

The galaxy’s circular velocity can be estimated from the image separation of  $0''.971$ . For an intrinsically spherical dark matter halo with a flat rotation curve (a singular isothermal sphere, or SIS), the image separation is given by  $\Delta\theta = 4\pi(v_c/c)^2 D_{ls}/D_{os}$ , where  $v_c$  is the circular velocity, and  $D_{ls}$  and  $D_{os}$  are (respectively) the lens–source and observer–source angular diameter distances. For the SIS model, the measured image separation corresponds to  $v_c = 264$  km s<sup>−1</sup>. For a thin Mestel disk, which also has a flat rotation curve,  $\Delta\theta = 8(v_c/c)^2 D_{ls}/D_{os}$  (Keeton, Kochanek, & Falco 1998), giving  $v_c = 331$  km s<sup>−1</sup>. The truth is probably between these two extremes.

With these figures, we find that the lens galaxy is compatible with the local Tully-Fisher relation as determined by Sakai et al. (2000). For the SIS model the lens galaxy is  $0.1 \pm 0.3$  mag brighter than predicted by the T-F relation, and for the Mestel model it is  $0.7 \pm 0.3$  mag fainter. The dispersion in the Sakai et al. (2000) T-F relation is 0.43 mag. These results indicate the lens galaxy appears to be a fairly normal spiral galaxy for its redshift.

An independent estimate of the lens galaxy’s circular velocity is available from the molecular absorption system detected by Wiklind & Combes (1998). They found absorption

lines at  $z_l = 0.886$  in front of SW, and also a weaker absorption line in front of NE shifted in rest-frame velocity by  $\Delta v = -147 \text{ km s}^{-1}$ . As they explained, the observed  $\Delta v$  can be used to estimate the circular velocity  $v_c$ , using the kinematic relation

$$\Delta v = v_c(\cos \theta_1 - \cos \theta_2) \sin i, \quad (1)$$

where  $i$  is the inclination, and  $\theta_k$  is the angle between the line of sight  $k$  (either NE or SW) and the line of nodes (as measured in the plane of the galaxy). The angles  $\theta_k$  are related to the corresponding sky-plane angles  $\phi_k$  by

$$\tan(\phi_k) = \tan(\theta_k) \sec i. \quad (2)$$

Using these relations, Wiklind & Combes (1998) used the data and models existing at the time to postulate that the lens galaxy is seen at low inclination ( $i < 20^\circ$ ) and is quite massive, and the quasar is at high redshift ( $z > 3$ ). These postulates have been proven broadly correct by our data and by the measured quasar redshift ( $z = 2.507$ ).

We can now update their determination of  $v_c$  using the new data. We must borrow a few results from the lens models that will be described later in § 4.1, namely, the inclination of the lens galaxy ( $i = 25^\circ$ ) and the orientation of the line of nodes ( $86^\circ \pm 3^\circ$ ). From these values and the measured galaxy position, we derive  $\phi_{\text{NE}} = 52^\circ$  and  $\phi_{\text{SW}} = 146^\circ$ . The resulting circular velocity is  $v_c = 255 \text{ km s}^{-1}$ . The corresponding Tully-Fisher magnitude is  $M_B = -21.5$ , which agrees well with the value inferred from the HST photometry ( $-21.7 \pm 0.3$ ).

## 4. The lens galaxy position and the Hubble constant

### 4.1. Updated lens models

In the most recent modeling effort for this system, Lehar et al. (2000) demonstrated a strong correlation between the position of the lens galaxy, which was poorly known, and the inferred value of  $H_0$ . Our measurement of the position of G allows us to determine  $H_0$  with much higher precision. At this stage we consider simple models constrained only by the positions of NE, SW, and G, and the magnification ratio (and not by the faint Einstein ring, which we leave for a future undertaking).

We modeled the lens galaxy as a singular isothermal ellipsoid using software written by Keeton (2001a). With as many parameters as constraints, the fits were exact. We estimated the error in each parameter to be the spread in the results obtained by allowing the position of G to vary through the full range of its quoted uncertainty. The results are given in Table 3.



Using this model and the time delay measured by Lovell et al. (1998), we obtain  $h = 0.44 \pm 0.09$  (where  $H_0 = 100h \text{ km s}^{-1} \text{ Mpc}^{-1}$ ), with most of the quoted uncertainty due to the 20% fractional uncertainty in the time delay. This value was computed assuming  $\Omega_m = 0.3$  and  $\Omega_\Lambda = 0.7$ , but the dependence on the cosmological model is weak; for  $\Omega_\Lambda = 0$  the result is  $h = 0.46$ . Either value is significantly lower than the Key Project value of  $0.72 \pm 0.08$  (Freedman et al. 2001), and also lower than several previous estimates of  $H_0$  from this system. In the rest of this section we discuss possible systematic modeling errors; in the next section we compare our model with previous work.

Our simple model might misrepresent the true mass distribution, in several ways. First, if there is an unmodeled source of convergence  $\kappa$  (due to, say, a nearby group of galaxies), then the inferred  $h$  is systematically low by the factor  $1 - \kappa$  (see, e.g., Gorenstein, Shapiro, & Falco 1988). Lehár et al. (2000) identified 4 galaxies besides the lens galaxy within  $20''$  of PKS 1830–211, which would contribute a convergence as high as  $\kappa = 0.16$  if they all lie at the lens redshift  $z_l = 0.886$ —although, in the following section, we argue that the nearest of these galaxies is probably at  $z_a = 0.19$  where it has a much smaller effect ( $\kappa \sim 0.03$ ).

Second, if the radial mass distribution is not isothermal, the inferred  $h$  is biased. If the lens potential  $\phi \propto r^\beta$  then the true  $h$  is  $(2 - \beta)$  times the isothermal estimate of  $h$  (Witt, Mao, & Keeton 2000). A similar bias results if the isothermal profile is truncated outside a radius comparable to, or smaller than, the Einstein ring radius. As a demonstration we modeled the lens galaxy as a pseudo-Jaffe ellipsoid ( $\rho \propto r^{-2}(r^2 + a^2)^{-2}$ ; see, e.g., Keeton 2001a) with a break radius  $a$ . For  $r \ll a$ , the pseudo-Jaffe profile has a flat rotation curve, but for  $r \gg a$  it has a Keplerian fall-off. We fixed  $a$  and allowed all other parameters to vary; the resulting  $h$  rises significantly for  $a < b$ , where  $b$  is the Einstein ring radius. Figure 3 shows the dependence of the inferred Hubble constant on the break radius.

However, in order to match the Key Project value of  $H_0$ , both of the preceding possibilities require unnatural parameters for the lens galaxy, which we have established is an apparently normal, massive, spiral galaxy. To obtain  $h = 0.72$  would require  $\beta = 0.36$ ; or, using the pseudo-Jaffe model,  $a/b = 0.38$ , corresponding to  $a = 0''.42 = 2.3h^{-1}$  kiloparsecs, at the lens redshift (assuming a flat  $\Omega_m = 0.3$  cosmology). Nearby massive spiral galaxies have flat rotation curves out to well beyond the visible extent of the spiral arms (see, e.g., Rubin, Thonnard, & Ford 1978; Sofue & Rubin 2001). In the *I*-band image, the spiral arms of the lens galaxy are detected out to a radius of at least  $0''.6 = 3.3h^{-1}$  kpc.

Third, our simple models may misrepresent the angular structure of the mass distribution, in addition to the radial structure. To investigate this possibility we computed a 2-d grid of models consisting of an SIE embedded in an external shear field. The ellipticity of the SIE was stepped from 0.0 to 0.2 (a plausible maximum value, given the nearly face-on

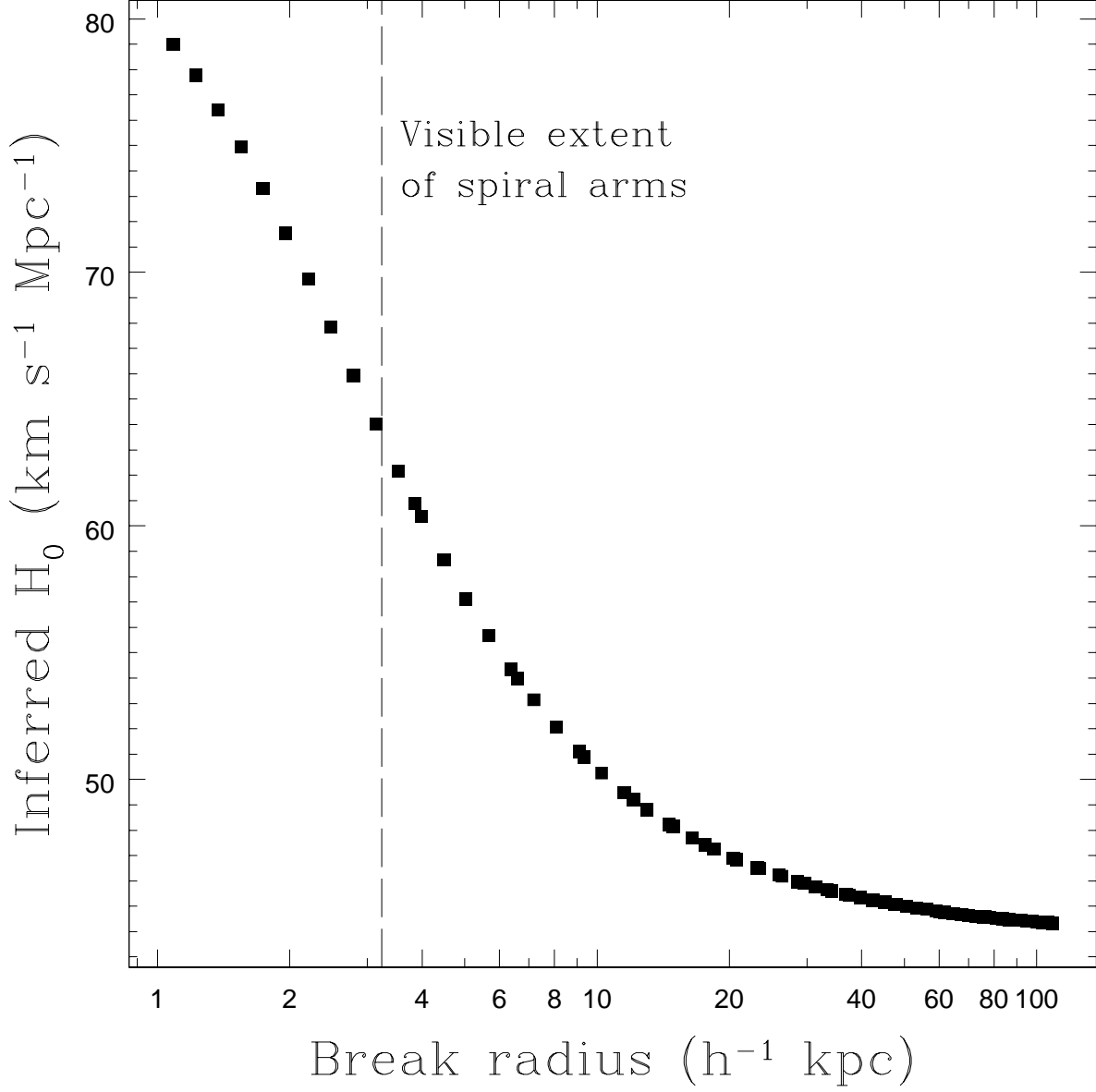


Fig. 3.— Variation of the inferred  $H_0$  with the break radius  $a$  in the pseudo-Jaffe model. The visible extent of the spiral arms is also marked. The horizontal scale has been set by the conversion factor  $5.4h^{-1}$  kpc per arcsecond, based on a flat  $\Omega_m = 0.3$  cosmology.

morphology), and its position angle was stepped from  $0^\circ$  to  $180^\circ$ , and in each case the corresponding parameters of the external shear field were determined. The resulting range in  $h$  was 0.33–0.55. The range in  $h$  widens, but the inferred  $h$  is not systematically large or small.

Fourth, a number of authors have recently argued that some lens galaxies have small-scale mass substructure (on scales  $< 10^9 M_\odot$ ) that smooth parameterized lens models fail to describe (see, e.g., Dalal & Kochanek 2001; Keeton 2001b; Bradac et al. 2001; Metcalf & Zhao 2001). The evidence lies in the discrepancy between measured and model-predicted flux ratios, which depend on the local curvature of the lens potential and are therefore sensitive to perturbations on small angular scales. This raises the possibility that the magnification ratio assumed for PKS 1830–211 may be grossly in error. However, the time delay does not depend strongly on the assumed magnification ratio. In fact, for isothermal models, Witt, Mao, & Keeton (2000) showed the time delay can be written purely as a function of the image positions.

Finally, there is the possibility raised by Courbin et al. (2002) that there is a second lens galaxy within the Einstein ring, which would obviously invalidate our single-galaxy model. We discuss this possibility further in § 5.

## 4.2. Comparison to previous models

There have been several previous attempts to model PKS 1830–211, most of which differ substantially in the placement of the lens galaxy. Figure 4 is a chart of the lens positions assumed by various authors, overlaid upon a gray-scale representation of the same region from the HST *I*-band image. The filled square shows the position measured in this work. The variation in  $H_0$  with lens position (as implied by the SIE model) is shown with contours. This figure is an updated version of Figure 5b by Lehár et al. (2000).

Kochanek & Narayan (1992) invented an inversion algorithm, LensClean, that determines both the mass model and source structure of lenses with extended emission, and applied it to radio maps of PKS 1830–211, with no constraints on the lens galaxy position. The resulting lens galaxy position has a large uncertainty but agrees with the position we have derived from the HST *I*-band image.

Nair, Narasimha, & Rao (1993) used an oblate spheroidal density distribution and a complex set of constraints inspired by features of VLA maps at 8 GHz and 15 GHz. Following Subrahmanyam et al. (1990), they required the lens galaxy to be located near a faint radio component (“E”) that they argued is an additional image of the background

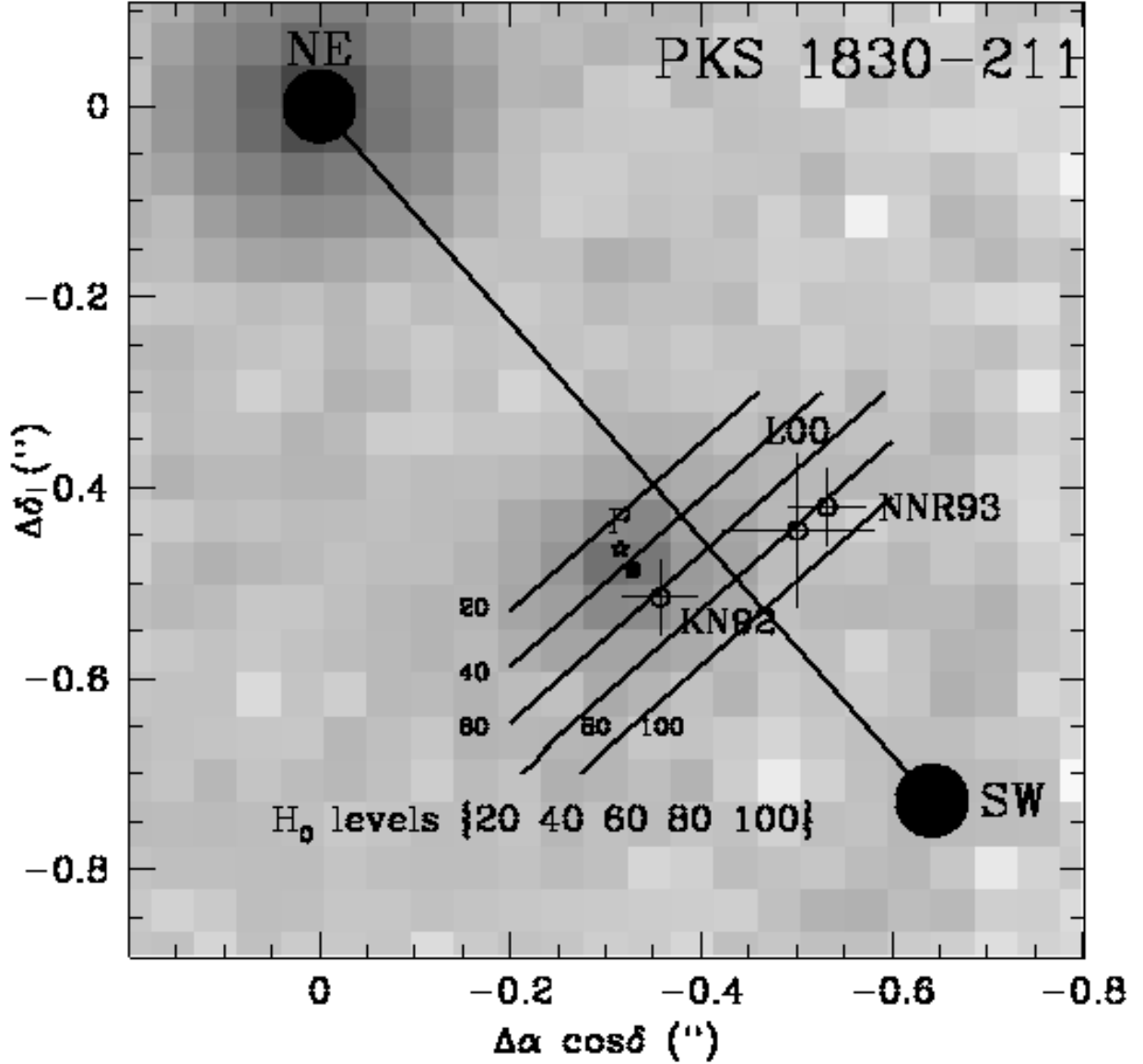


Fig. 4.— Variation of inferred  $H_0$  with lens galaxy position in the SIE model. This is an updated version of Figure 5b by Lehár et al. (2000). Plotted are the lens galaxy positions measured in this work (filled square) and by Lehar et al. (2000, labeled L00); and the model positions of Nair, Narasimha, & Rao (1993, NNR93) and Kochanek & Narayan (1992, KN92). The point P was identified by L00 (in an image with a lower signal-to-noise ratio) as either a foreground star or the bulge of G, and is here seen to be consistent with the bulge of G.

source or emission from the center of the lens galaxy. However, although the existence of E has been verified in other radio images, it is over  $0''.2$  away from the center of the lens galaxy as revealed by our HST image. In particular, the center of the lens galaxy and component E are on opposite sides of the line between A and B, corresponding to a qualitative difference in the lens models (see below).

All previous authors who have used PKS 1830–211 to determine the Hubble constant chose a lens galaxy position close to the incorrect position of Nair, Narasimha, & Rao (1993). After measuring the time delay, Lovell et al. (1998) applied the model of Nair, Narasimha, & Rao (1993) to determine  $h = 0.65^{+16}_{-9}$ . Koopmans & Fassnacht (1999) obtained  $h = 0.75^{+18}_{-10}$  using an isothermal mass model in which the center of the lens galaxy was fixed at the value of Nair, Narasimha, & Rao (1993).

Lehár et al. (2000), who were the first to measure the lens galaxy position, obtained  $h = 0.73 \pm 0.35$  using an SIE model. The large uncertainty was due to the lens galaxy position, which was poorly constrained, but in agreement with the position of Nair, Narasimha, & Rao (1993). The difference between their result and ours can be attributed entirely to the updated position. In particular, we have assumed the pointlike object labeled “P” by Lehár et al. (2000) is actually the bulge of the lens galaxy. Lehár et al. (2000) noted this possibility, but for their analysis they assumed that P was a foreground star. In an independent analysis, Courbin et al. (2002) argue that there is indeed a spiral lens galaxy but that P is a foreground star superimposed nearly on the bulge of the galaxy; this possibility is discussed further in § 5.

Lehár et al. (2000) favored a scenario in which the nearby galaxy G2 is an  $L_*$  galaxy located at the lens redshift  $z_l = 0.886$ . They noted that the major axis in their SIE model pointed towards G2, suggesting G2 could naturally explain the ellipticity of the mass model. By representing G and G2 as singular isothermal spheres, they achieved a satisfactory fit, and the resulting ratio of Einstein ring radii ( $b_{G2}/b_{G1} = 0.7 \pm 0.4$ ) was consistent with the nearly equal  $H$ -band magnitudes and scale lengths of the galaxies.

The new data provide two reasons to reject this interpretation. First, after moving the lens galaxy to the correct position, the major axis in the updated SIE model points  $91^\circ$  away from G2—exactly the wrong direction for G2 to explain the ellipticity. Consequently, when we recalculated the SIS+SIS model,  $b_{G2}$  converged to zero.

Second, the  $VI$  images show that G2 is a spiral galaxy that is larger in angular size, higher in surface brightness, and bluer than G, all of which suggest that G2 is at lower redshift. By summing within the apertures described in § 2 we find that the mean surface brightness of G2 is  $1.7 \pm 0.4$  times higher than that of G. After correcting for Galactic

extinction<sup>7</sup>, we find for G2 that  $V - I = 0.94 \pm 0.28$ , as compared to  $V - I > 2$  for G. The blue  $V - I$  color of G2 is typical of spiral galaxies at either  $z < 0.3$  or  $z > 1.7$ , according to the spectrophotometric models computed by Lehár et al. (2000). For further comparison with those models, we computed the  $H$ -band magnitude of G2, by applying the aperture-photometry procedure described in § 2 to the image of Lehár et al. (2000). The result was  $H = 19.18 \pm 0.07$ , giving an extinction-corrected magnitude of 18.9. This places G2 in the  $z < 0.5$  section of the  $V - I/I - H$  plane (see Fig. 3 of Lehár et al. 2000).

Finally, we note that G2 is the only known candidate for the source of the  $z_a = 0.19$  H I absorption seen by Lovell et al. (1996). Together these facts lead us to favor a scenario in which G2 is located at  $z_a = 0.19$ . The extinction-corrected  $I$ -band magnitude of G2 is  $19.9 \pm 0.1$ , corresponding to  $\sim 0.07L_*$  for a spiral galaxy at  $z_a = 0.19$ . Such a small and relatively nearby galaxy would be irrelevant to lens models with the present degree of accuracy, contributing a tidal shear and convergence  $\gamma \sim \kappa \sim 0.03$ .

One argument against this scenario is that the absorption feature detected by Lovell et al. (1996) was seen primarily in front of NE, even though SW is closer in projection to G2 ( $2''.5$  vs.  $2''.0$ ). However, given the peculiar and patchy distribution of H I on kiloparsec scales seen in some nearby galaxies (see, e.g., Hibbard et al. 2001), we do not view this as a serious complication.

## 5. Summary and future prospects

The new HST  $I$ -band image confirms that the lens galaxy of PKS 1830–211 is a nearly face-on spiral galaxy. Assuming that the compact component near the center of this galaxy is the galaxy bulge, we have accurately measured the galaxy position relative to the quasar images, thereby completing the basic data for this system.

Furthermore, we have computed  $H_0$  given the current best measurement of the time delay, assuming that there is only one lens galaxy, and further assuming that the lens galaxy has a flat rotation curve and a massive dark halo, as appears to be the case for nearby massive spiral galaxies. The resulting  $H_0$  is lower than the widely accepted value obtained by the Key Project. We have described some possible sources of bias, but to force agreement with the Key Project seems to require an unnatural mass model for the lens galaxy.

After this work was done, we learned that Courbin et al. (2002) independently analyzed

---

<sup>7</sup>The corrections were computed using the  $E_{B-V}$  value of Schlegel, Finkbeiner, & Davis (1998) and assuming a  $R_V = 3.1$  extinction law; the results are  $A_V = 1.4$ ,  $A_I = 0.81$ , and  $A_H = 0.27$ .

the same HST data as presented in § 2 (along with the *IHK* data of Lehar et al. (2000) and a new Gemini *K*-band image). The main difference between their treatment of the *VI* data and ours is that they deconvolved the images before interpreting them. Their interpretation differs from ours in two important respects:

1. Courbin et al. (2002) conclude object P is a foreground star rather than the bulge of the face-on spiral galaxy. In support of this claim, P is unresolved and its position in a color-magnitude diagram is consistent with other bulge dwarf stars for this field. Based on the mean density of field stars that were detected in the *I*-band image ( $\sim 0.8 \text{ arcsec}^{-2}$ ), there is a 10% chance for a randomly placed star to lie within  $0''.2$  of the center of the galaxy. The photometry is also consistent with a spiral galaxy with P as its bulge (see § 3), so both interpretations are reasonable.
2. Courbin et al. (2002) conclude there is a second lens galaxy, based on faint and extended flux between P and the SW quasar that is detected only in the *H*-band image of Lehar et al. (2000). Its position is rather uncertain (with a quoted error of 80 mas) but is consistent with the position of radio component E. In this scenario, the *H*-band flux and component E are due to a second deflector that is radio-loud. In our scenario, these features (if they are real, and not associated with the quasar) could be due to star formation in the western spiral arm of lens galaxy.

In short, our interpretation has the virtue of simplicity. The interpretation of Courbin et al. (2002) is complicated but has the merit of explaining a few puzzling features of the data: a possible offset between P and the center of the spiral arms, the diffuse *H*-band flux, and radio component E. It is not clear to us, from the present data, how seriously these features should be taken.

If P is indeed a star, the lens galaxy position we report in this paper is wrong. Adopting the position of Courbin et al. (2002) and the SIE model described in § 4.1, the inferred Hubble constant would rise to  $H_0 = 107 \pm 30 \text{ km s}^{-1}$ . If, however, there is a second galaxy between the quasar images, then it may be impossible to determine  $H_0$  from this system because the galaxies would be difficult to characterize with current telescopes, and the mass model would be complex. In particular it is not possible to state generally (without detailed modeling) whether a two-deflector model would alleviate or exacerbate the incompatibility of the Key Project value of  $H_0$  and the time delay measured for this system.

Therefore, for the purpose of determining  $H_0$  with this system, the highest priority should be establishing which of these competing hypotheses are correct. It would be difficult to establish the identity of P via spectroscopy, because P is faint and the field is crowded.

But, as Courbin et al. (2002) pointed out, it would be possible to prove P is a star by measuring its proper motion, which should be  $\sim 4 \text{ mas yr}^{-1}$  for a bulge star (for which the solar reflex motion of  $\sim 200 \text{ km s}^{-1}$  is dominant). A negative result would not be conclusive. The reality of the second deflector might be tested by seeking to detect both deflectors in a single image—perhaps a considerably deeper *I*-band image with the HST’s new Advanced Camera for Surveys.

Assuming for the moment that our interpretation of the HST images is correct, we suggest the following steps to reduce the systematic errors and sharpen the determination of  $H_0$  from this system.

First, the uncertainty in the time delay should be reduced from 20% to 3% or lower, so that it makes no significant contribution to the overall uncertainty. Lovell et al. (1998) noted that their full light curves were consistent with a broad range of time delays, ranging from 12 to 30 days. Only when the data were restricted to a subset containing a single “bump” did the distribution of possible time delays become approximately Gaussian. A time delay based on multiple features in a full set of light curves would be more secure.

Second, the redshift of galaxy G2 ( $I = 20.7$ ) needs to be measured spectroscopically to test whether it is the source of the  $z_a = 0.19$  H I absorption. The plausibility of the association with G2 could also be checked by mapping the H I absorption with a higher signal-to-noise ratio than the map of Lovell et al. (1996), in order to search for absorption in front of SW, and to measure any velocity shift.

Third, and most important, the degeneracies of lens models must be broken by making use of more observational constraints than the basic data presented in Table 1. For example, we did not investigate realistic models for spiral galaxies that include contributions from the bulge, disk, and halo (see, e.g., Keeton & Kochanek 1998; Koopmans et al. 1998). More generally, many authors have argued that unless a wide class of parameterized models are considered (e.g., Kochanek 1991; Bernstein & Fischer 1999), or even a non-parametric model (e.g., Williams & Saha 2000), the uncertainty in  $H_0$  will be underestimated. To investigate a broader range of models, more constraints are obviously required. For the simple models described in § 4, we have ignored two possible sources of such constraints: the milliarcsecond-scale radio morphologies of the quasar cores, and the Einstein ring.

The quasar cores have been mapped with very long baseline interferometry (VLBI) at radio frequencies ranging from 843 MHz to 43 GHz. Maps with angular resolution  $\gtrsim 10 \text{ mas}$  show the expected parity-reversed substructure in NE and SW (see, e.g., Jauncey et al. 1991; Patnaik & Porcas 1996), but maps with higher angular resolution are difficult to interpret. Component SW, at least, appears to be scatter-broadened by plasma in the lens galaxy



(Jones et al. 1996; Guirado et al. 1999). It has been claimed that both NE and SW exhibit intrinsic variability in source structure (Jin et al. 1999). Furthermore, NE has a  $\sim 10$  mas linear jet with no obvious counterpart in SW (Garrett et al. 1996; Guirado et al. 1999), which may indicate the presence of small-scale substructure in the lens. It is hard to see how the existing observations can be dramatically improved with current telescopes, but a modeling effort may help to determine whether mass substructure is required, and if so, whether the mass scale of the perturbation is large enough to affect the time delay.

The geometry of the Einstein ring is probably the best hope for breaking the remaining degeneracies of lens models. The situation is analogous to the case at optical wavelengths, where the stretched images of quasar host galaxies have been used to break some degeneracies in mass models of the time delay lens PG 1115+080 (Kochanek, Keeton, & McLeod 2001; although see Saha & Williams 2001). We have made some preliminary attempts to use the existing VLA maps for this purpose, by employing the curve-fitting algorithm of Keeton (2001a), but with the angular resolution of the present data it is difficult to measure the ring with the needed accuracy.

There is room for improvement upon existing radio maps of the ring, which tend to be short snapshots because the radio cores are so bright ( $\sim 3$  Jy). (In most of the VLBI observations, the ring is resolved out.) These snapshots are limited in dynamic range by poor sampling in Fourier space rather than thermal noise. Major improvements would follow from deep radio observations with high angular resolution ( $< 0''.1$ ) and high dynamic range ( $> 10^5$ ). Methods for the precise interpretation of high-dynamic-range interferometric observations of lensed sources are well developed and have been shown to discriminate between different mass models (see, e.g., Kochanek & Narayan 1992; Kochanek 1995; Chen, Kochanek, & Hewitt 1995; Ellithorpe, Kochanek, & Hewitt 1996).

We thank Aaron Cohen and Jim Lovell for help with this research. We are grateful to Steven Beckwith for providing Director’s Discretionary time for this project. This work was partially supported by NASA through grants DD-8804, GO-7495, and GO-9133 from the Space Telescope Science Institute. J.N.W. is supported by an NSF Astronomy and Astrophysics Postdoctoral Fellowship.

## REFERENCES

- Bernstein, G. & Fischer, P. 1999, *AJ*, 118, 48
- Bond, J.R., et al. 1994, *Phys. Rev. Lett.*, 72, 13

- Bradac, M., et al. 2001, preprint, astro-ph/0112038
- Chen, G., Kochanek, C.S., & Hewitt, J.N. 1995, ApJ, 447, 62
- Courbin, F., et al. 1998, ApJ, 499, 119
- Courbin, F., et al. 2002, submitted (astro-ph/0202026)
- Dalal, N. & Kochanek, C.S. 2001, preprint (astro-ph/0111456)
- Djorgovski, S., et al. 1992, MNRAS, 257, 240
- Dolphin, A. 2000, PASP, 112, 1397
- Eisenstein, D.J., Tegmark, M., & Hu, W. 1998, ApJ, 504, 57
- Ellithorpe, J.D., Kochanek, C.S., & Hewitt, J.N. 1996, ApJ, 464, 556
- Falco, E.E., et al. 1999, ApJ, 523, 617
- Freedman, W., et al. 2001, ApJ, 553, 47
- Fruchter, A. & Hook, R.N. 2002, PASP, in press (astro-ph/9808087)
- Frye, B., Welch, W.J., & Broadhurst, T. 1997, ApJ, 478, 25
- Garrett, M.A., et al. 1996, in Proc. IAU Symp. 173, Astrophysical Applications of Gravitational Lensing, ed. C.S. Kochanek & J.N. Hewitt (Dordrecht: Kluwer), p. 189
- Gerin, M., et al. 1997, ApJ, 488, 31
- Gorenstein, M.V., Shapiro, I.I., & Falco, E.E. 1988, 327, 693
- Guirado, J.C., et al. 1999, A&A, 346, 392
- Hibbard, J.E., et al. 2001, to appear in ASP Conf. Series Vol. 240, Gas and Galaxy Evolution, eds. J.E. Hibbard, M.P. Rupen, & J.H. van Gorkom (San Francisco: ASP), 659 (astro-ph/0110667)
- Jauncey, D.L., et al. 1991, Nature, 352, 132
- Jin, C., et al. 1999, New Astronomy Reviews, 43, 767
- Jones, D.L., et al. 1996, ApJ, 470, 23
- Keeton, C.R. & Kochanek, C.S. 1998, ApJ, 495, 157

- Keeton, C.R., Kochanek, C.S., & Falco, E.E. 1998, *ApJ*, 509, 561
- Keeton, C.R. 2001a, preprint, astro-ph/0102340
- Keeton, C.R. 2001b, preprint, astro-ph/0111595
- Kochanek, C.S. 1991, *ApJ*, 373, 354
- Kochanek, C.S. 1995, *ApJ*, 445, 559
- Kochanek, C.S., Keeton, C.R., & McLeod, B.A. 2001, *ApJ*, 547, 50
- Kochanek, C.S. & Narayan, R. 1992, *ApJ*, 401, 461
- Koopmans, L.V.E., et al. 1998, *MNRAS*, 295, 534
- Koopmans, L.V.E. & Fassnacht, C.D. 1999, *ApJ*, 527, 513
- Krist, J.E. & Hook, R.N. 1997, *The Tiny Tim User's Guide*, version 4.4 (Baltimore: STScI)
- Lehár, J., et al. 2000, *ApJ*, 536, 584
- Lidman, C., et al. 1999, *ApJ*, 514, 57
- Lovell, J.E.J., et al. 1996, *ApJ*, 472, 5
- Lovell, J.E.J., et al. 1998, *ApJ*, 508, 51
- Metcalf, R. & Zhao, H. 2001, preprint, astro-ph/0111427
- Nair, S., Narasimha, D., & Rao, A.P. 1999, *ApJ*, 407, 46
- Patnaik, A.R. & Porcas, R.W. 1996, in *Proc. IAU Symp. 173, Astrophysical Applications of Gravitational Lensing*, ed. C.S. Kochanek & J.N. Hewitt (Dordrecht: Kluwer), p. 305
- Rao, A. & Subrahmanyam, R. 1988, *MNRAS*, 231, 229
- Refsdal, S. 1964, *MNRAS*, 128, 307
- Riess, A. 2000, *Instrument Science Report WFPC2 00-04* (Baltimore: STScI)
- Rubin, V.C., Thonnard, N., & Ford, W.K. Jr. 1978, *ApJ*, 225, 107
- Sakai, S., et al. 2000, *ApJ*, 529, 698
- Saha, P. & Williams, L. 2001, *AJ*, 122, 585

- Schechter, P.L. 2000, to be in Proc. IAU Symp. 201, New Cosmological Data and the Values of the Fundamental Parameters, ed. A.N. Lasenby & A. Wilkinson (San Francisco: ASP)
- Schlegel, D.J., Finkbeiner, D.P., & Davis, M. 1998, *ApJ*, 500, 525
- Sofue, Y. & Rubin, V. 2001, *ARA&A*, 39, 137
- Subrahmanyan, R., et al. 1990, *MNRAS*, 246, 263
- Swift, J.J., Welch, W.J., & Frye, B.L. 2001, *ApJ*, 549, 29
- Tully, R.B. & Fisher, J.R. 1977, *A&A*, 54, 661
- Vogt, N., et al. 1996, *ApJ*, 465, 15
- Vogt, N., et al. 1997, *ApJ*, 479, 121
- Wiklind, T. & Combes, F. 1996, *Nature*, 379, 139
- Wiklind, T. & Combes, F. 1998, *ApJ*, 500, 129
- Williams, L. & Saha, P. 2000, *AJ*, 119, 439
- Witt, H.J., Mao, S., & Keeton, C.R. 2000, *ApJ*, 544, 98
- Wu, X.-P., et al. 1995, *ApJ*, 448, 65
- Ziegler, B.L., et al. 2001, preprint (astro-ph/0111146)

Table 1. Basic data for PKS 1830–211

Datum	Value	Reference
R.A.(NE) (J2000)	18 <sup>h</sup> 33 <sup>m</sup> 39 <sup>s</sup> .931	Subrahmanyan et al. (1990)
Decl.(NE) (J2000)	−21°03′39″.75	Subrahmanyan et al. (1990)
R.A.(SW) – R.A.(NE)	−642 ± 1 mas	Jin et al. (1999)
Decl.(SW) – Decl.(NE)	−728 ± 1 mas	Jin et al. (1999)
R.A.(G) – R.A.(NE)	−328 ± 4 mas	this work
Decl.(G) – Decl.(NE)	−486 ± 4 mas	this work
NE/SW magnification ratio	1.52 ± 0.05	Lovell et al. (1998)
Lens redshift ( $z_l$ )	0.886 ± 0.001	Wiklind & Combes (1998)
Source redshift ( $z_s$ )	2.507 ± 0.002	Lidman et al. (1999)
Time delay ( $t_{\text{SW}} - t_{\text{NE}}$ )	26 <sup>+4</sup> <sub>−5</sub> days	Lovell et al. (1998)

<sup>a</sup>Wiklind & Combes (1998) measured molecular absorption lines at redshifts 0.88582 in front of SW, and also an absorption line in front of NE with a rest-frame velocity shift of −147 km s<sup>−1</sup>.

Table 2. HST/WFPC2 photometry

Component	F814W $\approx I$	F555W $\approx V$
S1	19.33 ± 0.04	21.90 ± 0.18
NE	21.97 ± 0.05	25.8 ± 0.2
SW	> 24.9	> 26.3
G	22.04 ± 0.25	≥ 24.7
G2	20.69 ± 0.13	22.24 ± 0.25

Table 3. SIE model parameters

Parameter	Value
Einstein ring radius ( $b$ )	0″.491 ± 0.001
Ellipticity ( $\epsilon$ )	0.091 ± 0.009
P.A. of major axis (E of N)	86° 1 ± 3° 1
$x_{\text{source}} - x_{\text{NE}}$	−0″.264 ± 0″.005
$y_{\text{source}} - y_{\text{SW}}$	−0″.418 ± 0″.005
Magnification of NE	5.9 ± 0.6